Formation and Stability of μ_2-Peroxo on Titanosilicates, Anatase and Rutile: Implications for Zeotype Catalysts

Lukas Lätsch,[†] Imke B. Müller,[‡] Christoph J. Kaul,[†] Trees De Baerdemaeker,[‡] Andrei-Nicolae Parvulescu,[‡] Karsten Seidel,[‡] J. Henrique Teles,[‡] Natalia Trukhan,[‡] Christophe Copéret[†,*]

[†] ETH Zurich, Department of Chemistry and Applied Biosciences, Vladimir-Prelog Weg 2, Zurich, Switzerland
[‡] BASF SE, Ludwigshafen, Germany

ABSTRACT: Extra-framework TiO_2 in titanosilicate oxidation catalysts has generally been linked with low selectivity and great emphasis has been put on developing synthetic protocols that yield anatase-free materials. Here, using ^{17}O solid-state NMR spectroscopy, we investigate the formation and stability of μ_2-peroxo groups on both titanosilicates containing or not containing extra-framework TiO_2 as well as TiO_2 polymorphs. By comparison with TiO_2 nanoparticle references, H_2O_2 activation (e.g. peroxo formation) and decomposition is proposed to be related to the presence of rutile-like extra-framework TiO_2. In fact, μ_2-peroxo species can form and remain stable on anatase, whereas they decompose quickly on rutile. According to DFT calculations, the high stability of μ_2-peroxo surface species on anatase is due to the specific arrangement of μ_2-oxo groups on the (101) surface that allows for stabilization of key-intermediates through H-bonding. Notably, the μ_2-peroxo species formed on titanosilicates and anatase display distinct ^{17}O NMR spectroscopic signatures, that relates directly to the Ti coordination environments, and can thus be distinguished.

INTRODUCTION

Titanosilicates are a class of heterogenous catalysts where highly dispersed Ti(IV) sites are embedded in a crystalline SiO_2 matrix.[1] They have attracted great interest in both industry and academia due to their ability to catalyze a number of selective oxidation reactions with H_2O_2, leaving only water as the byproduct.[2] For example, Ti-zeotypes catalyze the epoxidation of propylene, the ammoximation of cyclohexanone and methylethylketone and the hydroxylation of phenol.[3–6] Since the discovery of TS-1 *ca.* 40 years ago,[7] researchers sought to improve catalyst performance through synthesis of Ti zeotypes with novel framework architecture yielding larger pore sizes (MWW, BETA, MOR, …)[2] or through post-synthetic modification introducing meso-porosity (hierarchical zeotypes).[8–10] On a molecular level, a great challenge has been to relate the presence of specific sites to catalytic performances. Over the years, besides the classical framework-incorporated tetrahedral Ti,[11] a multitude of sites have been proposed to be beneficial or detrimental, including extra-framework TiO_2, penta- and octahedral defects as well as partially hydrolyzed sites.[12–15] Non-isolated sites have mostly been linked with limited selectivity as well as H_2O_2 decomposition. As H_2O_2 is a rather expensive primary oxidant,[16] limiting its non-productive decomposition has been a focus of research, by, for instance developing synthetic protocols to avoid the formation of so-called extra-framework TiO_2.[17–19] Although widely accepted,[9,20–22] recent studies have challenged the generality of this assumption showing that anatase extra-framework TiO_2 can also be beneficial.[23–25]

In addition, our group has recently shown that μ_2-peroxo groups are formed on paired Ti sites upon contact with H_2O_2, based on their ^{17}O solid-state NMR (ssNMR) signatures and comparison with molecular analogues.[26] Their formation and stability were proposed to be related to catalytic performances. DFT calculations suggest that these peroxo sites correspond to off-cycle reaction intermediates, but that upon activation with a second H_2O_2 molecule highly reactive hydroperoxo species are generated due to H-bonding with the zeolitic framework.[27,28] At present, little is known regarding the possible formation and stability of the corresponding peroxo species on extra-framework TiO_2, even if peroxotitanium complexes[29] have been invoked as precursors in both anatase and rutile formation.[30,31] We thus decided to investigate the formation and the stability of μ_2-peroxo groups on TiO_2 polymorph themselves and a family of titanosilicates with different content of extra-framework TiO_2 using ^{17}O ssNMR spectroscopy as a methodology to identify peroxo species.[27] Firstly, we establish that the stability of μ_2-peroxos does in fact correlate with hydrogen peroxide activation among titanosilicates. Next, we show that stable μ_2-peroxo groups can also form on anatase, while they are unstable on rutile leading to fast H_2O_2 decomposition. DFT calculations indicate that the origin of this reactivity difference lies in the specific surface structure of anatase (vs. rutile) and that the possible diagonal arrangement of μ_2-oxo

groups on the anatase (101) surface is a key structural feature that enables the stabilization of these peroxo intermediates through H-bonding.

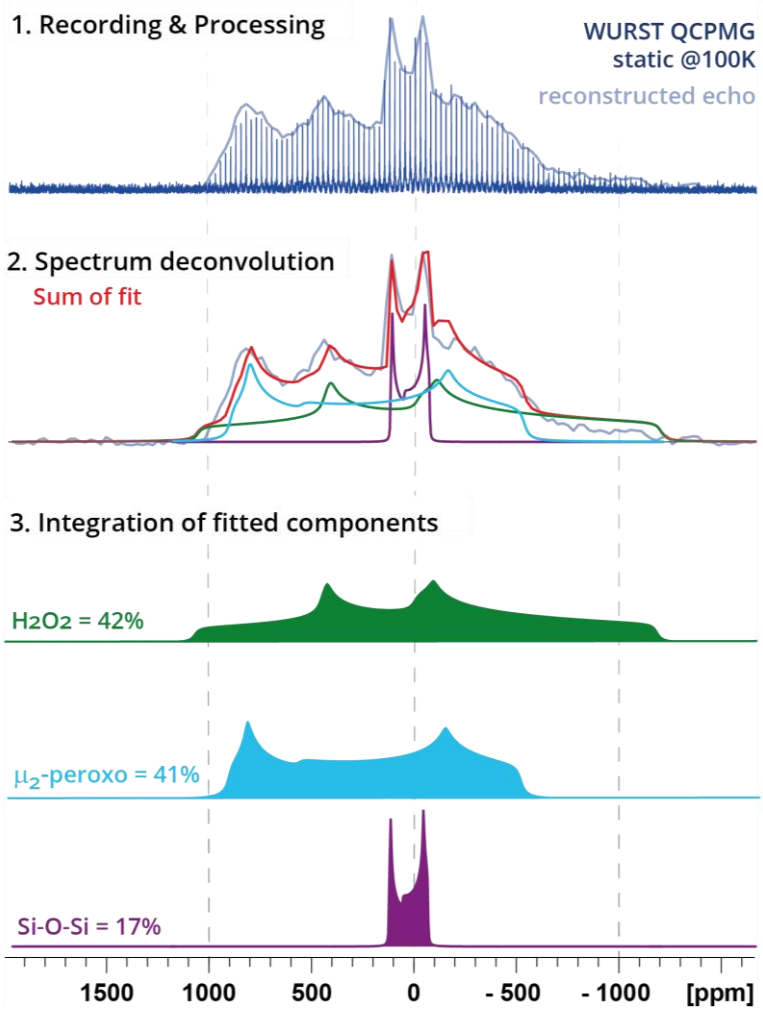

Figure 1: Overview over developed methodology. 1) ^{17}O NMR WURST QCPMG of a TS-1 contacted with $H_2{}^{17}O_2$ and reconstructed echo-spectrum. 2) Site deconvoluted spectra with up to three species present: H_2O_2 (green), μ_2-peroxo (blue) and Si-O-Si (purple). Sum of fit shown in red. 3) Relative amount of each species obtained via ratio of integrated signals.

RESULTS

We first decided to establish a quantification protocol to assess the formation and stability of μ_2-peroxos on titanosilicates and TiO_2. Upon contact with an aqueous solution of $H_2{}^{17}O_2$ (*ca.* 1 M, H_2O unlabeled, details see ESI Ch. S1.1) up to three species can be detected in ^{17}O ssNMR spectroscopy: unreacted H_2O_2, the μ_2-peroxo and labeled oxygen incorporated in siloxane bridges, Si-O-Si,[32,33] resulting from the reaction of the framework with labeled H_2O formed upon decomposition of H_2O_2 (see Fig. 1). Note that all spectra were recorded at 100 K to avoid decomposition, increase sensitivity and freeze out dynamics

during the recording of NMR spectra. As ^{17}O is a quadrupolar nuclei, each signal is defined by 8 parameters (relating to the chemical shift tensor (δ_{iso}, Ω, κ), the electric field gradient tensor (C_Q, η) and the associated Euler angles (α, β, γ)), which have to be fitted individually to avoid overfitting (for the obtained parameters of H_2O_2 and H_2O on SiO_2 see ESI Ch. S3.1 and Tab. S1). If the contact time after impregnation of $H_2{}^{17}O$ on SiO_2 is sufficiently prolonged (> 2 days), the same Si-O-Si ^{17}O NMR signal appears that is visible directly after decomposition of the μ_2-peroxo groups (see ESI Fig. S13), indicating that H_2O_2 can enter into the pores substantially faster than H_2O at ambient conditions. For TS-1, if impregnated with $H_2{}^{17}O$, we observe a small signal at 360 ppm in addition, which is attributed to oxygen incorporated adjacent to the Ti (Si-O-Ti).[34]

The NMR parameters (δ_{iso}, Ω, κ, C_Q, η, α, β, γ) associated with each individual signal (see ESI Tab. S1) are next used in a three-step quantification protocol. First, following acquisition, the echo spectrum is reconstructed from the measured WURST QCPMG spectrum (used to improve sensitivity)[35] in order to obtain a continuous lineshape. Next, the lineshape is fitted using the dmfit software package, by only allowing the respective intensities of H_2O_2, μ_2-peroxo and Si-O-Si signals to vary (the parameters obtained from the individual signals are used for all titanosilicates studied herein to increase the overall robustness of the approach).[36] Finally, the relative concentrations of the three species were obtained through integration (see Fig. 1).

With this protocol in hands, we looked at four titanosilicates: TS-1 A having no extra-framework TiO_2 (see ESI for characterization details), and TS-1 B, TiMWW A & B all having extra-framework TiO_2 as evidenced from Ti-O-Ti scattering pathways in the Ti K edge XANES white-line region (see ESI Fig. S5 & S6). To evaluate the selectivity of the four titanosilicates we performed a standardized test to assess the rate of decomposition of H_2O_2 (pseudo-first order, performed at 80°C, see ESI Ch. S2.3 for details). Analyzing the pseudo-1st-order H_2O_2 decomposition rates at 80°C obtained with TS-1 A ($k = 0.43\ h^{-1}$) and TS-1 B ($k = 0.16\ h^{-1}$), we notice that TS-1 B displays a low rate, despite having extra-framework TiO_2 present. For TiMWW A ($k = 0.01\ h^{-1}$) and TiMWW B ($k = 0.14\ h^{-1}$), we observe a difference of an order of magnitude, with TiMWW A showing a similar (low) rate compared to the blank experiment with no catalyst. In comparison, when contacted with 1 equiv. of H_2O_2 per Ti, TS-1 A shows fast formation and high stability of the μ_2-peroxo and TS-1 B shows slow formation and high stability of the μ_2-peroxo. TiMWW A shows slow formation of the μ_2-peroxo and overall the slowest consumption of H_2O_2 even after 2 h of contact time. TiMWW B shows slow formation and low stability of the μ_2-peroxo (see Fig. 2). The lower fraction of μ_2-peroxo initially formed by TS-1 B and both TiMWW can be explained with the presence of extra-framework TiO_2 as some of the Ti is inaccessible. This effect is largest for TiMWW A, in line with the most dominant white-line features in Ti K edge XANES (see ESI Fig. S6).

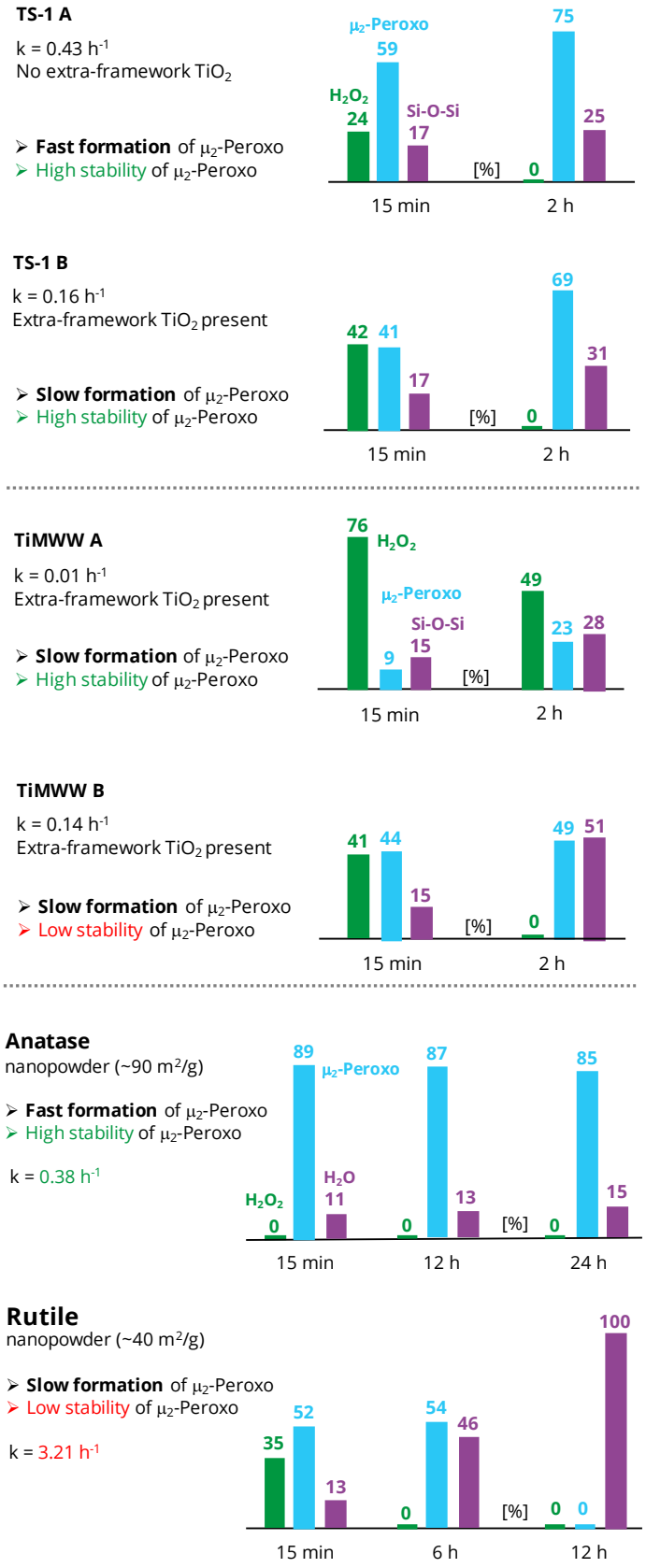

Figure 1: Bar plot comparison of relative amount of H_2O_2, μ_2-peroxo and Si-O-Si/H_2O formed for TS-1 A/B and TiMWW A/B after initial exposure to aqueous solution of $H_2{}^{17}O_2$ and after 2h of contact, respectively and for anatase and rutile nanoparticles after initial exposure to aqueous solution of $H_2{}^{17}O_2$ and prolonged contact times (12h and 24h for anatase, 6h and 12h for rutile nanoparticles).

Interestingly, the stability of the μ_2-peroxo correlates with selectivity of the catalyst: high peroxo stability correlates with low H_2O_2 decomposition rates (TS-1 A & TS-1 B) and *vice versa* (TiMWW A *vs.* TiMWW B). TS-1 B, TiMWW A & B having all extra-framework TiO_2 show very different μ_2-peroxo stability and H_2O_2 decomposition rates. One possible explanation for such behavior could be that the extra-framework TiO_2 of the respective catalysts differ in their nature. Indeed, closer inspection of the Ti K edge XANES white-line region and comparison with anatase and rutile nanoparticles references indicates that the extra-framework TiO_2 present in TS-1 B and TiMWW A is anatase-like (peak at 4987 eV, see ESI Fig. S5 & S6) and rutile-like in the TiMWW B (peak at 4992 eV).

So far, the μ_2-peroxo has only been invoked on framework or framework associated sites,[27,28] but could in principle also form on the surface of (extra-framework) TiO_2. We thus investigated the formation and stability of μ_2-peroxos on anatase and rutile nanoparticle references (for details see ESI S1.4). Impregnation was adjusted to reach a maximum surface coverage of *ca.* 4 peroxo/nm^2. Surprisingly, the μ_2-peroxo groups not only form very quickly on anatase, but also display very high stability (see Fig. 2). Even after 24 h of impregnation, only 15% have decomposed into H_2O. Notably, the μ_2-peroxo signal displays a slightly smaller C_Q on TiO_2 than on TS-1, *vide infra*), indicating that they have different environment. In sharp contrast, the μ_2-peroxos form significantly more slowly on rutile and fully decompose within 12 h. These findings parallel the decomposition rate of H_2O_2 on titanosilicates with anatase- and rutile-like extra-framework TiO_2: while the measured rate for anatase is comparable with titanosilicates free of extra-framework TiO_2 ($k = 0.38\ h^{-1}$, see ESI Ch. 2.3), rutile displays a significantly faster decomposition, which is one order of magnitude higher ($k = 3.21\ h^{-1}$).

Discussion

In order to understand the difference in decomposition rates of adsorbed H_2O_2 on rutile and anatase, we performed periodic DFT calculations. We selected the (101) and the (110) surfaces for anatase and rutile, respectively, because they are the most abundant surface for each polymorph.[37] Both facets expose μ_2-O and μ_3-O, as well as penta- and hexa-coordinated Ti (see Fig. 3a & b).[38,39] While H_2O_2 adsorption is favorable on the rutile (110) surface (-85 kJ/mol) and subsequent formation of a μ_2-peroxo is possible (-7 kJ/mol, -9 kJ/mol for the *trans*-peroxo), further cleavage or decomposition of the adsorbed H_2O_2 is highly exothermic (-111 kJ/mol, see Fig. 3c), consistent with the possible formation and low stability of the peroxo species as observed experimentally by ^{17}O NMR. Adsorption of H_2O_2 on the anatase (101) surface is also favored (-56 kJ/mol), but contrary to (110) rutile surface, cleavage of the O-O bond is not energetically favorable (see Fig. 3d). A key difference between these two surfaces across these polymorph is the arrangement of the μ_2-O atoms: whereas they are linearly arranged on the (110) rutile surface, they

are arranged in a diagonal fashion on the (101) anatase surface.[37–39] Proton transfer from the adsorbed H_2O_2 to one adjacent μ_2-O leads to the formation of a surface hydroxyl moiety and a μ_2-OOH, where the hydroperoxo is stabilized through H-bonding with the OH moiety (-50 kJ/mol), which possibly helps avoiding decomposition. Furthermore, this arrangement allows for a second proton transfer, yielding a *trans*-Ti-peroxo and adsorbed water (-94 kJ/mol). The latter can then rearrange to a stable μ_2-peroxo (-106 kJ/mol).

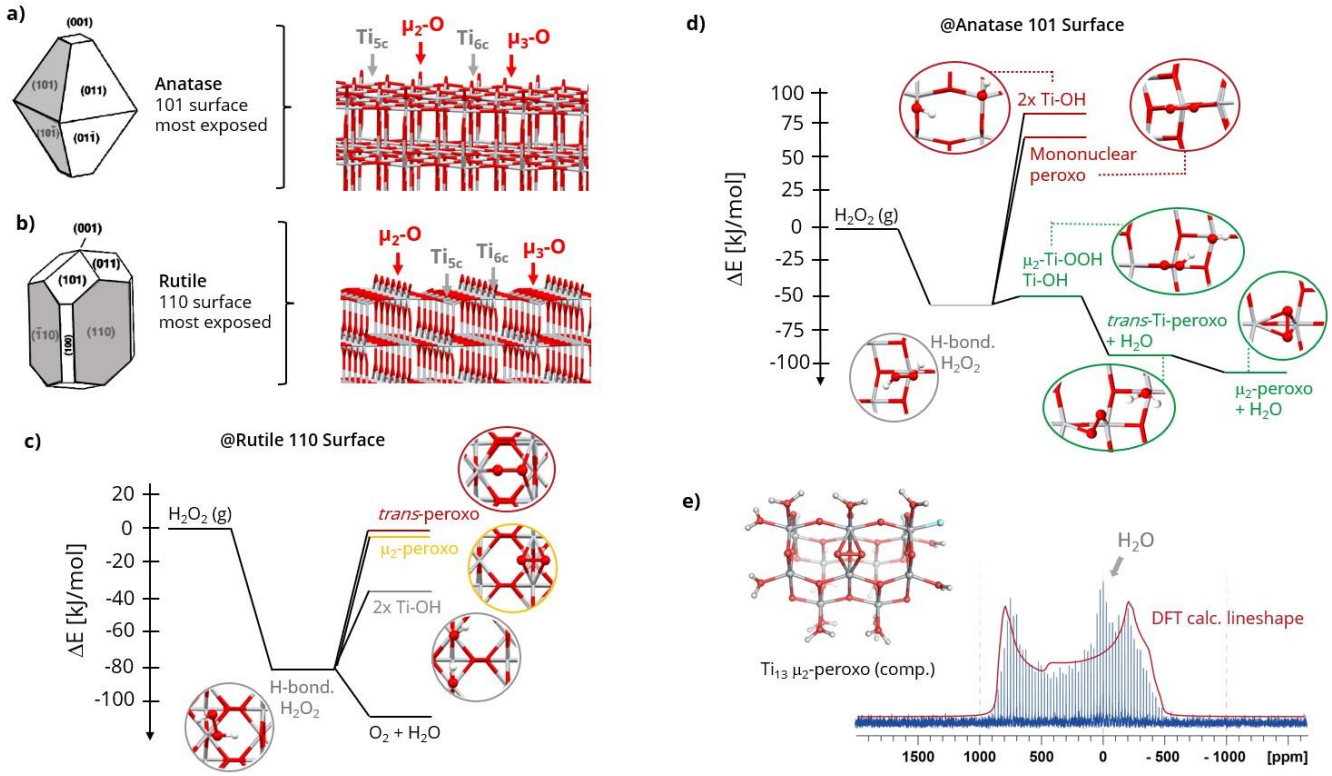

Figure 3: Computational analysis of peroxo formation on anatase and rutile surface. Wulff construction of anatase (a) and rutile (b) nanoparticles and their most exposed surfaces, respectively (adapted from ref [40]). c) Decomposition of H_2O_2 on rutile (110) surface. d) Pathway towards stable μ_2-peroxo on anatase (101) surface. e) Extracted peroxo surface model and calculated ^{17}O NMR spectroscopic signature.

We subsequently extracted a cluster model of the μ_2-peroxo (Ti_{13}-cluster, see Fig. 3e) to compute the ^{17}O NMR spectroscopic signature for comparison with the measured spectrum. The calculated lineshape matches almost perfectly with the experimental NMR signatures on anatase. The observed and calculated C_Q (~15 MHz) is significantly smaller than the observed one on TS-1 (~17 MHz). We thus decided to investigate the effect of the coordination number on Ti (number of oxygen atoms coordinating to Ti) on C_Q and computed three different molecular systems based on $[Ti_2O(O_2)(acac)_{2x}(OiPr)_{2(2-x)}]$, with x=0,1,2, as a model system for a neutral Ti sites in various coordination environments. The calculated DFT values show a C_Q of 16.7 MHz for x=0 (parent Ti system 4 coordinated), that decreases to 16.3 MHz for x=1 (parent Ti system 5 coordinated) and 15.3 MHz for x=2 (parent Ti system 6 coordinated). These results

indicate that bridging μ_2-peroxos can have significantly different spectroscopic signatures depending on Ti coordination, *e.g.* the higher the coordination the lower the C_Q and *vice versa*. These findings parallel what is observed experimentally: the larger C_Q of the μ_2-peroxo found in TS-1 & TiMWW compared to anatase is consistent with a bridging peroxo species on Ti sites with lower coordination than the six-fold coordination found in anatase as expected for framework Ti.

Conclusion

We have developed a robust method to quantify the ease of formation and relative stability of μ_2-peroxo groups on titanosilicates such as industrially relevant catalysts TS-1 and TiMWW, as well as TiO_2 based on solid-state ^{17}O NMR spectroscopy. Application of this method on a titanosilicate library highlights significant differences in both the formation rate and the stability, that we could link not only with presence of extra-framework TiO_2, but with its specific structure. Notably, rutile-like TiO_2 leads to unstable μ_2-peroxo groups that translates into fast H_2O_2 decomposition under catalytic conditions. In contrast, anatase-like TiO_2 yields very stable μ_2-peroxo groups owing to diagonally arranged μ_2-Os that stabilize key intermediates through H-bonding. These findings show that the presence of TiO_2 does not have to be detrimental to selectivity as previously often assumed, but that it depends on the type of TiO_2, rutile being particular efficient to decompose H_2O_2. Many studies have centered around synthesizing extra-framework TiO_2-free titanosilicates,[17–19] however, especially for hierarchical zeolites this can often not be avoided.[8,10] Our findings suggest that in such cases more focus should lie on the modification of the TiO_2, that could lead to its "passivation". Overall, we show that solid-state ^{17}O NMR spectroscopy augmented by computational studies is a powerful approach to explain performance of heterogenous catalysts on the molecular level, ultimately yielding new ideas for further catalyst design.

AUTHOR INFORMATION

Corresponding Authors
* Christophe Copéret: ccoperet@ethz.ch.

CONFLICT OF INTEREST
The authors declare that they have no conflict of interest.

ACKNOWLEDGMENT
L.L. thanks the Scholarship Fund of the Swiss Chemical Industry (SSCI) and BASF for funding. The author thanks SynMatLab for financial support of our NMR facility. C.J.K. acknowledges the Swiss National Science Foundation (SNF IZLCZ0_206049). The Swiss Norwegian beamlines (SNBL, ESRF) are acknowledged for provision of beamtime through proposal 31-01-143. We thank Dr. W. van Beek and Dr. D. Stoian for their support during XAS experiments. We thank Dr. Christopher P. Gordon, Dr. Laura Piveteau, Dr. Zachariah J. Berkson, Dr. Alexander V. Yakimov and Laura A. Völker for helpful discussions.

REFERENCES

(1) Smeets, V.; Gaigneaux, E. M.; Debecker, D. P. Titanosilicate Epoxidation Catalysts: A Review of Challenges and Opportunities. *ChemCatChem* **2022**, *14* (1), 1–26. https://doi.org/10.1002/cctc.202101132.

(2) Xu, H.; Wu, P. Recent Progresses in Titanosilicates New Titanosilicates With Novel Crystal- Line Structures. **2017**. https://doi.org/10.1002/cjoc.201600739.

(3) Romano, U.; Esposito, A.; Maspero, F.; Neri, C.; Clerici, G. M. Selective Oxidation with Ti-Silicalite. *Chim.Ind.(Milan)*. 1990, p 610.

(4) Lin, M.; Xia, C.; Zhu, B.; Li, H.; Shu, X. Green and Efficient Epoxidation of Propylene with Hydrogen Peroxide (HPPO Process) Catalyzed by Hollow TS-1 Zeolite: A 1.0 Kt/a Pilot-Scale Study. *Chem. Eng. J. (Amsterdam, Neth.)* **2016**, *295*, 370–375. https://doi.org/10.1016/j.cej.2016.02.072.

(5) Ge, Q.; Lu, J.; Zhu, M. *Research Progress of Titanium Silicalite Molecular Sieve for Cyclohexanone Ammoximation*; Hecheng Xianwei Gongye: 38(1), 54-58, 2015.

(6) Li, M.; Liu, J.; Na, H. *Application and Advancements in Synthesis of 2-Butanone Oxime*; Huaxue Gongchengshi: 20(7), 42-43, 2006.

(7) Taramasso, M.; Perego, G.; Notari, B. *US4410501A*; 1983.

(8) Sanz, R.; Serrano, D. P.; Pizarro, P.; Moreno, I. Hierarchical TS-1 Zeolite Synthesized from SiO2 TiO2 Xerogels Imprinted with Silanized Protozeolitic Units. *Chem. Eng. J.* **2011**, *171* (3), 1428–1438. https://doi.org/10.1016/j.cej.2011.02.036.

(9) Zhang, T.; Chen, X.; Chen, G.; Chen, M.; Bai, R.; Jia, M.; Yu, J. Synthesis of Anatase-Free Nano-Sized Hierarchical TS-1 Zeolites and Their Excellent Catalytic Performance in Alkene Epoxidation. *J. Mater. Chem. A* **2018**, *6* (20), 9473–9479. https://doi.org/10.1039/c8ta01439f.

(10) Weissenberger, T.; Leonhardt, R.; Zubiri, B. A.; Pitínová-Štekrová, M.; Sheppard, T. L.; Reiprich, B.; Bauer, J.; Dotzel, R.; Kahnt, M.; Schropp, A.; Schroer, C. G.; Grunwaldt, J. D.; Casci, J. L.; Čejka, J.; Spiecker, E.; Schwieger, W. Synthesis and Characterisation of Hierarchically Structured Titanium Silicalite-1 Zeolites with Large Intracrystalline Macropores. *Chem. - A Eur. J.* **2019**, *25* (63), 14430–14440. https://doi.org/10.1002/chem.201903287.

(11) Lätsch, L.; Kaul, C. J.; Yakimov, A. V.; Müller, I. B.; Hassan, A.; Perrone, B.; Aghazada, S.; Berkson, Z. J.; De Baerdemaeker, T.; Parvulescu, A.-N.; Seidel, K.; Teles, J. H.; Copéret, C. NMR Signatures and Electronic Structure of Ti Sites in Titanosilicalite-1 from Solid-State 47/49 Ti NMR Spectroscopy. *J. Am. Chem. Soc.* **2023**, *145* (28), 15018–15023. https://doi.org/10.1021/jacs.2c09867.

(12) Guo, Q.; Sun, K.; Feng, Z.; Li, G.; Guo, M.; Fan, F.; Li, C. A Thorough Investigation of the Active Titanium Species in TS-1 Zeolite by in Situ UV Resonance Raman Spectroscopy. *Chem. - A Eur. J.* **2012**, *18* (43), 13854–13860. https://doi.org/10.1002/chem.201201319.

(13) Zuo, Y.; Liu, M.; Zhang, T.; Hong, L.; Guo, X.; Song, C.; Chen, Y.; Zhu, P.; Jaye, C.; Fischer, D. Role of Pentahedrally Coordinated Titanium in Titanium Silicalite-1 in Propene Epoxidation. *RSC Adv.* **2015**, *5* (23), 17897–17904. https://doi.org/10.1039/C5RA00194C.

(14) Signorile, M.; Braglia, L.; Crocellà, V.; Torelli, P.; Groppo, E.; Ricchiardi, G.; Bordiga, S.; Bonino, F. Titanium Defective Sites in TS-1: Structural Insights by Combining Spectroscopy and Simulation. *Angew. Chemie - Int. Ed.* **2020**, *59* (41), 18145–18150. https://doi.org/10.1002/anie.202005841.

(15) Wang, J.; Chen, Z.; Yu, Y.; Tang, Z.; Shen, K.; Wang, R.; Liu, H.; Huang, X.; Liu, Y. Hollow Core–Shell Structured TS-1@S-1 as an Efficient Catalyst for Alkene Epoxidation. *RSC Adv.* **2019**, *9* (65), 37801–37808. https://doi.org/10.1039/C9RA07893B.

(16) Zhang, Q.; Tan, X.; Bedford, N. M.; Han, Z.; Thomsen, L.; Smith, S.; Amal, R.; Lu, X. Direct Insights into the Role of Epoxy Groups on Cobalt Sites for Acidic H2O2 Production. *Nat. Commun.* **2020**, *11* (1). https://doi.org/10.1038/s41467-020-17782-5.

(17) Liu, Y.; Wang, F.; Zhang, X.; Zhang, Q.; Zhai, Y.; Lv, G.; Li, M.; Li, M. One-Step Synthesis of Anatase-Free Hollow Titanium Silicalite-1 by the Solid-Phase Conversion Method. *Microporous Mesoporous Mater.* **2022**, *331* (September 2021), 111676. https://doi.org/10.1016/j.micromeso.2021.111676.

(18) Fan, W.; Duan, R. G.; Yokoi, T.; Wu, P.; Kubota, Y.; Tatsumi, T. Synthesis, Crystallization Mechanism, and Catalytic Properties of Titanium-Rich TS-1 Free of Extraframework Titanium Species. *J. Am. Chem. Soc.* **2008**, *130* (31), 10150–10164. https://doi.org/10.1021/ja7100399.

(19) Zhang, J.; Shi, H.; Song, Y.; Xu, W.; Meng, X.; Li, J. High-Efficiency Synthesis of Enhanced-Titanium and Anatase-Free TS-1 Zeolite by Using a Crystallization Modifier. *Inorg. Chem. Front.* **2021**, *8* (12), 3077–3084. https://doi.org/10.1039/d1qi00311a.

(20) Lin, D.; Zhang, Q.; Qin, Z.; Li, Q.; Feng, X.; Song, Z.; Cai, Z.; Liu, Y.; Chen, X.; Chen, D.; Mintova, S.; Yang, C. Reversing Titanium Oligomer Formation towards High-Efficiency and Green Synthesis of Titanium-Containing Molecular Sieves. *Angew. Chemie - Int. Ed.* **2021**, *60* (7), 3443–3448. https://doi.org/10.1002/anie.202011821.

(21) Alba-Rubio, A. C.; Fierro, J. L. G.; León-Reina, L.; Mariscal, R.; Dumesic, J. A.; López Granados, M. Oxidation of Furfural in Aqueous H2O2 Catalysed by Titanium Silicalite: Deactivation Processes and Role of Extraframework Ti Oxides. *Appl. Catal. B Environ.* **2017**, *202*, 269–280. https://doi.org/10.1016/j.apcatb.2016.09.025.

(22) Yu, Y.; Tang, Z.; Wang, J.; Wang, R.; Chen, Z.; Liu, H.; Shen, K.; Huang, X.; Liu, Y.; He, M. Insights into the Efficiency of Hydrogen Peroxide Utilization over Titanosilicate/H2O2 Systems. *J. Catal.* **2020**, *381*, 96–107. https://doi.org/10.1016/j.jcat.2019.09.045.

(23) Niu, C.; Yang, X.; Zhang, Q.; Zhang, Y.; Qin, X.; Tang, Y.; Wei, H.; Gao, X.; Liu, Y.; Wang, X.; Wen, Y.; Xiao, F. S. Enhanced Catalytic Activity and Catalyst Stability in Cyclohexanone Ammoximation by Introducing Anatase into TS-1 Zeolite. *Microporous Mesoporous Mater.* **2023**, *351* (January), 112467. https://doi.org/10.1016/j.micromeso.2023.112467.

(24) Liu, C.; Huang, J.; Sun, D.; Zhou, Y.; Jing, X.; Du, M.; Wang, H.; Li, Q. Anatase Type Extra-Framework Titanium in TS-1: A Vital Factor Influencing the Catalytic Activity toward Styrene Epoxidation. *Appl. Catal. A Gen.* **2013**, *459*, 1–7. https://doi.org/10.1016/j.apcata.2013.03.013.

(25) Wang, Y.; Wang, S.; Zhang, T.; Ye, J.; Wang, X.; Wang, D. Effect of Extra-Framework Titanium in TS-1 on the Ammoximation of Cyclohexanone. *Trans. Tianjin Univ.* **2017**, *23* (3), 230–236. https://doi.org/10.1007/s12209-017-0042-5.

(26) Engler, H.; Lansing, M.; Gordon, C. P.; Neudörfl, J.-M.; Schäfer, M.; Schlörer, N. E.; Copéret, C.; Berkessel, A. Olefin Epoxidation Catalyzed by Titanium–Salalen Complexes: Synergistic H 2 O 2 Activation by Dinuclear Ti Sites, Ligand H-Bonding, and π-Acidity. *ACS Catal.* **2021**, *11* (6), 3206–3217. https://doi.org/10.1021/acscatal.0c05320.

(27) Gordon, C. P.; Engler, H.; Tragl, A. S.; Plodinec, M.; Lunkenbein, T.; Berkessel, A.; Teles, J. H.; Parvulescu, A.-N.; Copéret, C. Efficient Epoxidation over Dinuclear Sites in Titanium Silicalite-1. *Nature* **2020**, *586* (7831), 708–713. https://doi.org/10.1038/s41586-020-2826-3.

(28) Bai, R.; Song, Y.; Lätsch, L.; Zou, Y.; Feng, Z.; Copéret, C.; Corma, A.; Yu, J. Switching between Classical/Nonclassical Crystallization Pathways of TS-1 Zeolite: Implication on Titanium Distribution and Catalysis. *Chem. Sci.* **2022**, *13* (36), 10868–10877. https://doi.org/10.1039/d2sc02679a.

(29) Schwarzenbach, G.; Muehlebach, J.; Mueller, K. Peroxo Complexes of Titanium. *Inorg. Chem.* **1970**, *9* (11), 2381–2390. https://doi.org/10.1021/ic50093a001.

(30) de Mendonça, V. R.; Lopes, O. F.; Avansi, W.; Arenal, R.; Ribeiro, C. Insights into Formation of Anatase TiO2 Nanoparticles from Peroxo Titanium Complex Degradation under Microwave-Assisted Hydrothermal Treatment. *Ceram. Int.* **2019**, *45* (17), 22998–23006. https://doi.org/10.1016/j.ceramint.2019.07.345.

(31) Nag, M.; Ghosh, S.; Rana, R. K.; Manorama, S. V. Controlling Phase, Crystallinity, and Morphology of Titania Nanoparticles with Peroxotitanium Complex: Experimental and Theoretical Insights. *J. Phys. Chem. Lett.* **2010**, *1* (19), 2881–2885. https://doi.org/10.1021/jz101137m.

(32) Clark, T. M.; Grandinetti, P. J.; Florian, P.; Stebbins, J. F. Correlated Structural Distributions in Silica Glass. *Phys. Rev. B - Condens. Matter Mater. Phys.* **2004**, *70* (6), 1–8. https://doi.org/10.1103/PhysRevB.70.064202.

(33) Ashbrook, S. E.; Davis, Z. H.; Morris, R. E.; Rice, C. M. 17O NMR Spectroscopy of Crystalline Microporous Materials. *Chem. Sci.* **2021**, *12* (14), 5016–5036. https://doi.org/10.1039/d1sc00552a.

(34) Bellussi, G.; Rigutto, M. S. Metal Ions Associated to the Molecular Sieve Framework: Possible Catalytic Oxidation Sites. *Stud. Surf. Sci. Catal.* **1994**, *85* (C), 177–213. https://doi.org/10.1016/S0167-2991(08)60768-5.

(35) Schurko, R. W. Ultra-Wideline Solid-State NMR Spectroscopy. *Acc. Chem. Res.* **2013**, *46* (9), 1985–1995. https://doi.org/10.1021/ar400045t.

(36) Massiot, D.; Fayon, F.; Capron, M.; King, I.; Le Calvé, S.; Alonso, B.; Durand, J. O.; Bujoli, B.; Gan, Z.; Hoatson, G. Modelling One- and Two-Dimensional Solid-State NMR Spectra. *Magn. Reson. Chem.* **2002**, *40* (1), 70–76. https://doi.org/10.1002/mrc.984.

(37) Bourikas, K.; Kordulis, C.; Lycourghiotis, A. Titanium Dioxide (Anatase and Rutile): Surface Chemistry, Liquid-Solid Interface Chemistry, and Scientific Synthesis of Supported Catalysts. *Chem. Rev.* **2014**, *114* (19), 9754–9823. https://doi.org/10.1021/cr300230q.

(38) Kashiwaya, S.; Morasch, J.; Streibel, V.; Toupance, T.; Jaegermann, W.; Klein, A. The Work Function of TiO2. *Surfaces* **2018**, *1* (1), 73–89. https://doi.org/10.3390/surfaces1010007.

(39) Tian, F. H.; Wang, X.; Zhao, W.; Zhao, L.; Chu, T.; Yu, S. Adsorption of 2-Propanol on Anatase TiO2 (101) and (001) Surfaces: A Density Functional Theory Study. *Surf. Sci.* **2013**, *616*, 76–84. https://doi.org/10.1016/j.susc.2013.05.005.

(40) Diebold, U. The Surface Science of Titanium Dioxide. *Surf. Sci. Rep.* **2003**, *48* (5–8), 53–229. https://doi.org/10.1016/S0167-5729(02)00100-0.